ISSN: 2229-7359 Vol. 11 No. 18s, 2025

https://theaspd.com/index.php

"Stress Redistribution and Deformation Behavior in Twin Tunnels: A Comparative Analysis of Intact and Jointed Rock Mass Under Sequential Excavation Condition"

Rajnish Kumar Tiwari^{1*}, Imran Ahmad Khan², R. K. Srivastava³

- ¹ Research Scholar, Department of Civil Engineering, Amity University, Madhya Pradesh, Gwalior, MP474020, India
- ² Assistant professor, Department of Civil Engineering, Amity University, Madhya Pradesh, Gwalior, MP474020, India
- ³ Prof. (Retd.) Civil Engineering Department, Motilal Nehru National Institute of Technology, Prayagraj, UP 211004, India

Abstract: This study investigates the stress redistribution and deformation behavior in twin horse-shoe shaped tunnels under sequential excavation conditions, comparing intact and jointed rock masses. Using finite element software RS2, the research evaluates the influence of pillar width-to-diameter ratios (W/D = 0.3, 0.6, 1.2) and in-situ stress conditions ($K_0 = 0.5, 1.0, 1.5$) on tunnel stability and surrounding rock mass behavior. The analysis incorporated elasto-plastic behavior using the Hoek-Brown failure criterion for rock mass and Barton's model for jointed rock strength characterization. Results reveal that lower W/D ratios (0.3) and higher K_0 values (1.5) significantly amplify deformation differences, particularly at critical locations such as the springing level on the pillar side and the center of the pillar zone, where differences exceed 900%. Conversely, higher W/D ratios (1.2) minimized interaction effects and deformation discrepancies. The jointed rock mass exhibits more pronounced deformations compared to intact rock, emphasizing the role of discontinuities in tunnel stability. The findings provide critical insights for optimizing tunnel design and construction practices in challenging geological conditions, ensuring structural integrity and minimizing ground settlements.

1. Introduction

Twin tunnels offer a transformative solution to India's traffic congestion by optimizing road networks and enhancing connectivity. In urban areas, projects like the Mumbai Metro Line 3 utilize underground tunnels to bypass congested surface roads, easing pressure on overcrowded streets. On highways, twin tunnels, such as the Chenani-Nashri Tunnel, enable smoother traffic flow, reducing travel time and fuel consumption. By separating opposing traffic streams, they minimize accidents and delays, while projects like the Zojila Tunnel ensure year-round connectivity in challenging terrains. Overall, twin tunnels improve traffic management, decongest roads, and enhance commuter efficiency, addressing India's growing transportation challenges effectively. But even with successful tunnel construction experiences, building a tunnel in close proximity is a difficult task [1-5]. Unexpected stress concentrations and surface subsidence brought on by tunnel excavations may cause fatalities as well as the collapse of superstructures [6-10].

As the behavior of tunnels is influenced by a variety of factors, including the in-situ stress conditions, the presence of discontinuities, and the interaction between adjacent tunnels [11,12]. Tunnel stability in jointed rock masses is heavily influenced by anisotropic deformations, with bedding and joint structures dictating failure modes. Numerical studies show roof settlement and "virtual block" separation in stratified rock, while jointed rock fails via rotation, sliding, and falling. Increased joint density extends plastic zones deeper, enhancing instability. Complex joint structures worsen rock mass instability, necessitating better support strategies for tunnel safety [13]. Traditional methods of analysis, such as empirical formulas and closed-form solutions, have been widely used in the past [14]. However, these methods often fail to capture the complex behavior of rock masses due to the presence of discontinuities leading to complex and anisotropic behavior of the rock mass [15-17]. Discontinuities, such as joints, fractures, faults, and bedding planes, significantly influence the mechanical properties and stability of the rock mass [18,19]. Traditional analytical and numerical models often assume isotropic behavior, which is not valid for jointed rock masses. This leads to inaccurate predictions of stress redistribution and deformations around underground openings [21-23]. Asano et al. (2003) proposed an observational control method for excavating adjacent mountain

ISSN: 2229-7359 Vol. 11 No. 18s, 2025

https://theaspd.com/index.php

tunnels, focusing on real-time monitoring to adjust construction procedures. Their approach emphasizes minimizing ground disturbances and ensuring stability by using measured displacements to optimize support systems. The study emphasized the effectiveness of adaptive excavation techniques in jointed rock masses [24].

Bhasin and Hoeg (1997) studied the behavior of multiple jointed rock masses and found that the strength and deformational behavior of the rock mass are controlled by the size of individual blocks [25]. Hoek and Brown (1988) proposed a non-linear failure criterion for rock masses, which considers the behavior of interlocking particles and the softening of the rock mass [29]. This criterion has been widely used in the analysis of underground openings, especially in jointed rock masses. However, the Hoek-Brown criterion does not consider the effect of the intermediate principal stress, which can be significant in some cases [20, 28, 29]. Barton (1995) proposed that the rock mass quality index (Q-value) plays a crucial role in the selection of numerical methods. For rock masses with a large number of discontinuities, the discontinuum approach is more appropriate [30]. Srivastava (1985) conducted elastic and elasto-plastic FEM analysis of two interacting circular tunnels using the Hoek-Brown yield criterion. The study considered different pillar widths and in-situ stress ratios and found that the interaction between tunnels significantly affects the stress distribution and deformations in the pillar zone [31].

Ghaboussi and Ranken (1977) conducted a two-dimensional plane strain FEM analysis of interacting tunnels and found that the shortening of the pillar width causes additional ground settlements [32]. Zhang et al. (2020) emphasized that stress redistribution in jointed rock masses is highly dependent on the orientation and persistence of discontinuities [3, 4]. Varma et al. (2019) demonstrated that progressive failure in jointed rock masses is influenced by joint stiffness, orientation, and in-situ stress conditions [35]. Qibin Lin et al. (2020) employed the discrete element method to analyze the mechanical response of a jointed rock mass containing double circular holes under uniaxial loading, revealing that joints significantly reduce peak strength and elastic modulus. Strength and stiffness exhibit a "U"-shaped trend with joint dip angle, reaching their lowest values at 30°, increasing joint spacing enhances mechanical properties. Crack coalescence and displacement field analyses demonstrate how interactions between holes and joints govern fracture propagation mechanisms under loading. The study underscores the critical influence of joint orientation and spacing on the stability of perforated rock masses [41]. Fan Xiang et al. [2018] investigated the failure behavior of intermittent jointed rocks using PFC2D, revealing that joint inclination angle and continuity factor govern crack coalescence patterns under compressive and shear loading. Numerical tests identified four compressive and three shear failure modes, each exhibiting distinct crack propagation paths influenced by joint geometry and loading conditions. Contact force evolution analysis showed that force concentration transitions from uniform to scattered distribution, explaining differences in fracture mechanisms between shear and compressive failure [42].

Numerical methods, such as the Finite Element Method (FEM), have become increasingly popular for analyzing the behavior of underground openings. FEM allows for the simulation of complex geological conditions, including non-homogeneous media, non-linear material behavior, and the presence of discontinuities [2,3,7]. Several researchers have used FEM to study the interaction between tunnels. It was found that the interaction between tunnels becomes negligible for pillar width to diameter ratios greater than 1.

Shen and Barton (1997) conducted a parametric study using the 2D Distinct Element Code (UDEC) to analyze the effect of joint spacing on the shape and size of the influenced zone around excavated tunnels. They found that the behavior of jointed rock masses is significantly influenced by the orientation and spacing of the joints [26]. Huang, X. et al. (2016) assessed various isotropic, elasto-plastic hardening models for geomaterials and developed convenient forms of yield criteria for use in FEM analysis [33].

Zhang et al. (2020) investigated the failure modes of tunnels in jointed rock masses using numerical models only to reveal that the presence of complex joint structures significantly affects the stability of tunnels, with failure occurring

ISSN: 2229-7359 Vol. 11 No. 18s, 2025

https://theaspd.com/index.php

through a combination of sliding, rotation, and falling mechanisms [4]. Their study highlighted the importance of considering joint orientation and spacing in the design of tunnel support systems.

Huang et al. (2016) developed a versatile strength theory for the elasto-plastic analysis of tunnel surrounding rock [5, 33]. They used the generalized nonlinear unified strength theory to deduce analytical solutions for the radius and stress of the plastic zone around tunnels. Their results showed that the intermediate principal stress coefficient has a significant effect on the plastic range and the magnitude of stress in the surrounding rock.

Franza and DeJong (2019) proposed a two-stage elasto-plastic analysis method for modeling tunneling-induced soil-structure interaction. Their method, incorporated into the ASRE computer program, considers horizontal and vertical ground movements, isolated or continuous foundations, and various structural configurations. The study demonstrated the effectiveness of the proposed method in predicting building responses to tunneling operations [1].

Varma et al. (2019) conducted an experimental and numerical study on the response of tunnels in jointed rock masses under dynamic loading. They used a shake table experiment to validate a UDEC model and performed a parametric study to investigate the effects of in-situ stress, joint stiffness, and joint orientation on tunnel stability. Their findings indicated that shallow tunnels are more prone to damage from dynamic loading, and joint orientation plays a critical role in tunnel deformation [2].

Studies suggest that simultaneous excavation may lead to higher stress interactions between tunnels, while sequential excavation can cause asymmetric deformations due to staged stress release. Understanding these behaviors is essential for optimizing support systems, minimizing ground settlements, and ensuring the safe and efficient construction of closely spaced tunnels in complex geological conditions. Therefore, a parametric study considering two dimensional plain strain analysis is conducted on twin horse shoe shaped tunnels focusing on the effect of order of excavation on deformation behavior of tunnels while taking different in-situ stress ratios (Ko), pillar widths ratio's (W/D) as other variables, with the help of RS2 which uses finite element approach. The present study focuses on the elasto-plastic analysis of twin horse-shoe shaped tunnels in jointed rock mass, with a specific emphasis on deformation values and yield zone patterns. By comparing the deformation and yield zone outcomes in sequential excavation scenario implemented on intact and jointed rock mass, the research aims to evaluate their impact on tunnel stability and surrounding rock mass behavior. The analysis will provide critical insights into stress redistribution, deformation mechanisms, and potential failure zones in jointed rock formations. This comparative approach will help identify the most effective excavation strategy to minimize deformations and ensure structural integrity. The findings will contribute to optimizing tunnel design and construction practices, particularly in challenging geological conditions, offering practical solutions for infrastructure projects in similar environments.

2. Methodology and Numerical Modeling

The numerical modelling and analysis of twin horse-shoe shaped tunnels in jointed rock mass were conducted using the finite element software RS2. The tunnels were modeled to represent typical geological conditions encountered in India, particularly in hydroelectric projects, railways, and highways. The tunnel cross-section was designed with a maximum height and width of 8.0 m, consistent with standard dimensions used in such projects. The depth of the tunnels from the ground surface was set at 250 m to simulate deep excavation conditions and to analyze the interaction effects between the two tunnels [31, 36].

To accurately model the infinite extent of the geological medium, the external boundary of the finite element discretization was fixed at four times the maximum width or height of the tunnels. This boundary was assumed to be rigid and fixed, with displacements and rotations restricted in both the x and y directions. This approach ensures that the boundary conditions do not influence the stress and deformation patterns around the tunnels [36].

The study investigated the interaction effects between the twin tunnels by considering three pillar width-to-diameter ratios (W/D = 0.3, 0.6, and 1.2). These ratios were chosen to evaluate the influence of sequence of excavation on

ISSN: 2229-7359 Vol. 11 No. 18s, 2025

https://theaspd.com/index.php

stress redistribution and deformation patterns. The finite element mesh consisted of three-noded triangular elements, with a finer mesh density near the tunnel boundaries and pillar regions where higher stress concentrations are expected. A coarser mesh was used in areas farther from the tunnels to optimize computational efficiency without compromising accuracy.

The rock mass was modeled under elasto-plastic conditions to capture its behavior under varying stress states. The original Hoek-Brown failure criterion was adopted for the analysis, as it is well-suited for tightly interlocked jointed rock masses. This criterion effectively captures the nonlinear behavior of rock masses controlled by angular rock pieces. Tunnels were assumed to be excavated sequentially in the analysis to study their interaction effects under elasto-plastic conditions (fig. 1 & 2).

$$RMR = GSI + A \tag{1}$$

Where "A" accounts for groundwater and joint orientation conditions, typically ranging from 5 to 15. According to Table 1 and Equation (1), the RMR value is determined to be 67. Furthermore, applying the Rock Mass Classification (RMR) system as proposed by Bieniawsi and using Table 1 for intact rock mass properties and Table 2 for the assumed geological properties of discontinuities—the Rock Quality Designation (RQD) is calculated as 74 [40].

$$RQD=100e^{0.1\lambda} (0.1 \lambda +1)$$
 (2)

Joint frequency has been evaluated to be 10 which yield average joint spacing to be 0.1 m. Therefore, shear and normal stiffness of joints have been calculated from Eq. (3) and Eq. (4) [38].

$$K_n = E_i E_m / L (E_i - E_m)$$
(3)

$$K_s = 1/K_n$$
 (4)

Where E_i = Intact rock modulus, E_m = rock mass modulus, K_s = Joint shear stiffness, K_n = joint normal stiffness and L= average joint spacing.

Accordingly, it has been estimated that the normal and shear stiffness of discontinuities are 83382.9 MPa/m and 8338.3 MPa/m, respectively.

In the present study Barton's model [30, 38, 39] is used to estimate the shear strength of rock discontinuities, such as joints and fractures. The model incorporates the roughness and compressive strength of the discontinuity, along with the basic friction angle of the rock surface. The shear strength (τ) of a discontinuity is given by [39].

$$\tau = \sigma_n tan \left(\varphi_b + JRC \cdot log_{10} \left(JCS / \sigma_n \right) \right)$$
 (5) Where,

 τ = Shear strength of the discontinuity

 σ_n = Normal stress acting on the discontinuity

 ϕ_b = Basic friction angle of the rock surface

JRC = Joint Roughness Coefficient (0 for smooth, 20 for very rough)

JCS = Joint Compressive Strength (often a fraction of intact rock strength)

Barton's model is widely applied in rock slope stability, tunneling, and mining, providing a practical way to assess the behavior of jointed rock masses under various stress conditions.

Therefore, using table 1&2, Barton equation angle of internal friction and cohesion comes out to be 36.3 degrees and 1.041 Mpa respectively.

ISSN: 2229-7359 Vol. 11 No. 18s, 2025

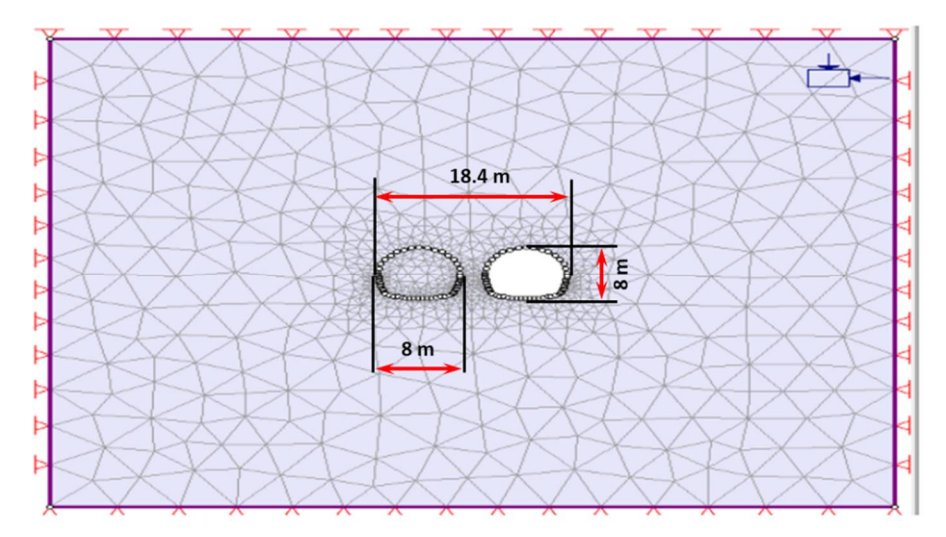


Fig. 1 Numerical model for stage1 of sequentially excavated horse shoe interacting tunnel section in intact rock with W/D = 0.3 and Ko = 1.5

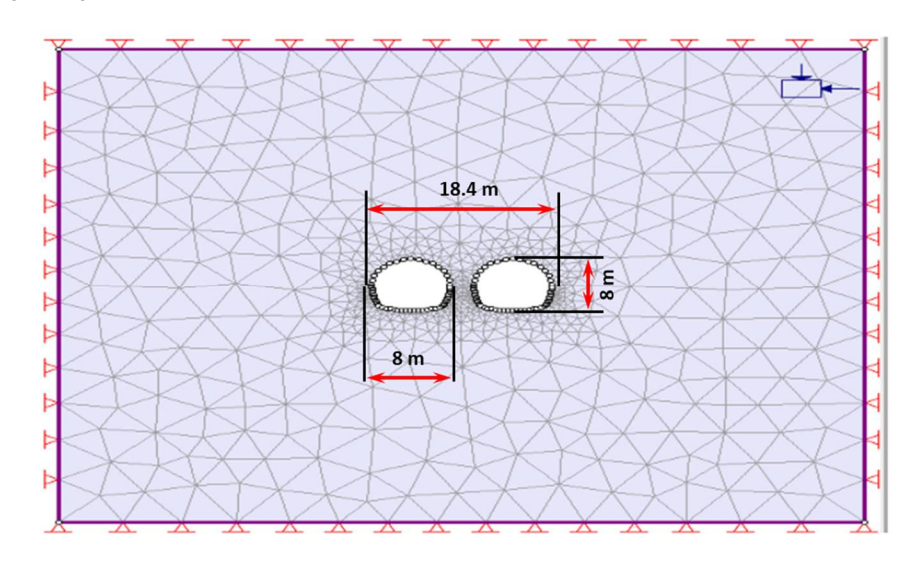


Fig. 2 Numerical model for stage 2 of sequentially excavated horse shoe interacting tunnel section in intact rock with W/D=0.3 and Ko=1.5

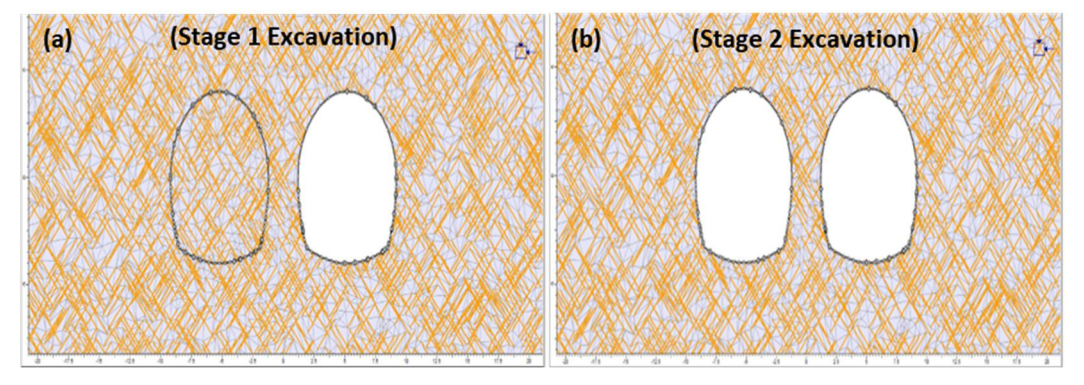


Fig. 3 Numerical model of sequentially excavated interacting tunnels in jointed rock mass with W/D = 0.3 and stress ratio of 1.5 Joint orientation = 45/45

ISSN: 2229-7359 Vol. 11 No. 18s, 2025

https://theaspd.com/index.php

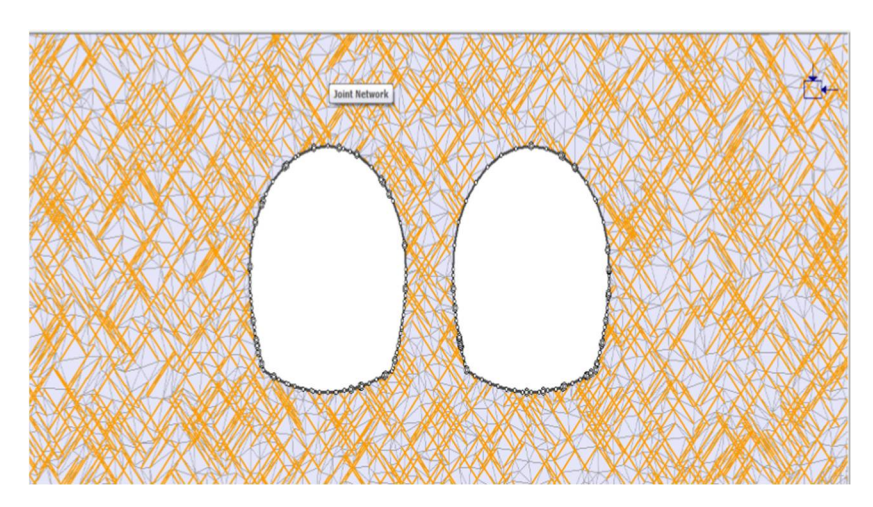


Fig. 4 Numerical model of interacting tunnels excavated sequentially in jointed rock mass with W/D = 0.3 and stress ratio of 1.5 Joint orientation = 45/45 (Enlarged View)

The field stress ratio (Ko), defined as the ratio of horizontal to vertical stress, was varied as 0.5, 1.0, and 1.5 to assess its influence on tunnel stability and deformation. These values were selected based on established approaches in rock mechanics literature. The vertical stress (σ_v) at the tunnel depth was calculated as 6.75 MPa, consistent with the overburden pressure at 250 m depth. The analysis incorporated these stress conditions to evaluate the stress redistribution and deformation patterns around the tunnels under different excavation scenarios.

Table 1: Geotechnical Properties of Intact Rock and Rock Mass

Value				
122.364 MPa				
0.2879 MPa				
35,000 MPa				
0.21				
0.028 MPa/m				
17				
62				
0.8				
6,734 MPa				
27.01				

ISSN: 2229-7359 Vol. 11 No. 18s, 2025

https://theaspd.com/index.php

Residual Hoek-Brown Constant (mb)	0.2206
Residual Hoek-Brown Constant (s)	0.00001575

Mohr-Coulomb Parameters		
Condition	Cohesion (c)	Friction Angle (φ)
Peak Values (K0 = 1.0 and 0.5)	1.752 MPa	48.34°
Peak Values (K0 = 1.5)	2.101 MPa	45.63°
Residual Values ($K0 = 1.0$ and 0.5)	0.8786 MPa	32.21°
Residual Values (K0 = 1.5)	1.1646 MPa	29.37°
Drucker-Prager Parameters		
Condition	q	k
Peak Values (K0 = 1.0 and 0.5)	0.5931	0.4905
Residual Values ($K0 = 1.0$ and 0.5)	0.747	0.7148
Peak Values (K0 = 1.5)	0.7657	0.533
Residual Values (K0 = 1.5)	1.4692	0.701

Table 2 Joint and discontinuous properties

Discontinuity sets	45/45
Discontinuity length	2m
Joint water pressure	not present
Persistence	0.2
Separation	<0.001 m
Infilling	None

3. Results and discussion

The analysis focuses on the impact of the width-to-depth (W/D) ratio on the deformation of the tunnels, considering both intact and jointed rock masses. The results are presented in terms of the percentage difference in deformation for various W/D ratios. Figures 5, 6 and 7 displays the contour diagrams showing the variation of displacements around interacting horse shoe tunnels in intact rock mass for different W/D ratios and Ko values,

ISSN: 2229-7359 Vol. 11 No. 18s, 2025

https://theaspd.com/index.php

whereas Figures 8, 9 and 10 display the contour diagrams showing the variation of displacements around interacting horse shoe tunnels in jointed rock mass for different W/D ratios and Ko values.

3.1 Discussion:

For left tunnel at JO 45-45:

1. At Springing Level on Pillar Side:

The deformation decreases as the W/D ratio increases from 0.3 to 1.2. For example, at W/D = 0.3, the deformation is 427.81, which decreases to 209.35 at W/D = 1.2. fig. 11(a). This indicates that the tunnel experiences less deformation at higher W/D ratios at the springing level on the pillar side.

2. At Invert Level on Abutment Side:

The deformation also decreases with increasing W/D ratio. At W/D = 0.3, the deformation is 50.99, which decreases to 41.21 at W/D = 1.2. Fig 11(d). This suggests that the invert level on the abutment side is less deformed at higher W/D ratios.

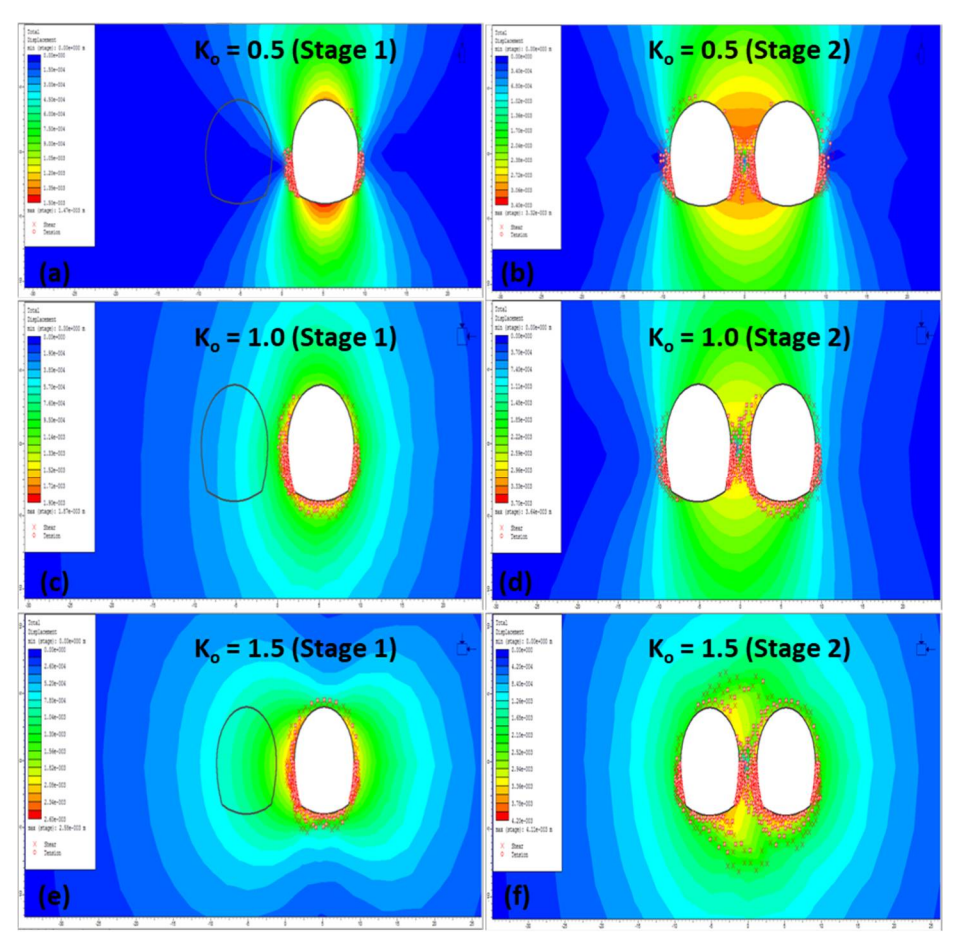


Fig. 5 Variation of displacements around interacting horse shoe tunnels in intact rock mass W/D 0.3

3. At Crown and Centre of Invert:

The deformation at the crown and centre of invert levels shows a decreasing trend with increasing W/D ratio. For example, at the crown, the deformation decreases from 43.81 at W/D = 0.3 to 23.94 at W/D = 1.2, fig. 11(b & e). This trend is consistent with the behavior observed at the springing level on the pillar side, indicating that the crown and invert levels are also less deformed at higher W/D ratios.

ISSN: 2229-7359 Vol. 11 No. 18s, 2025

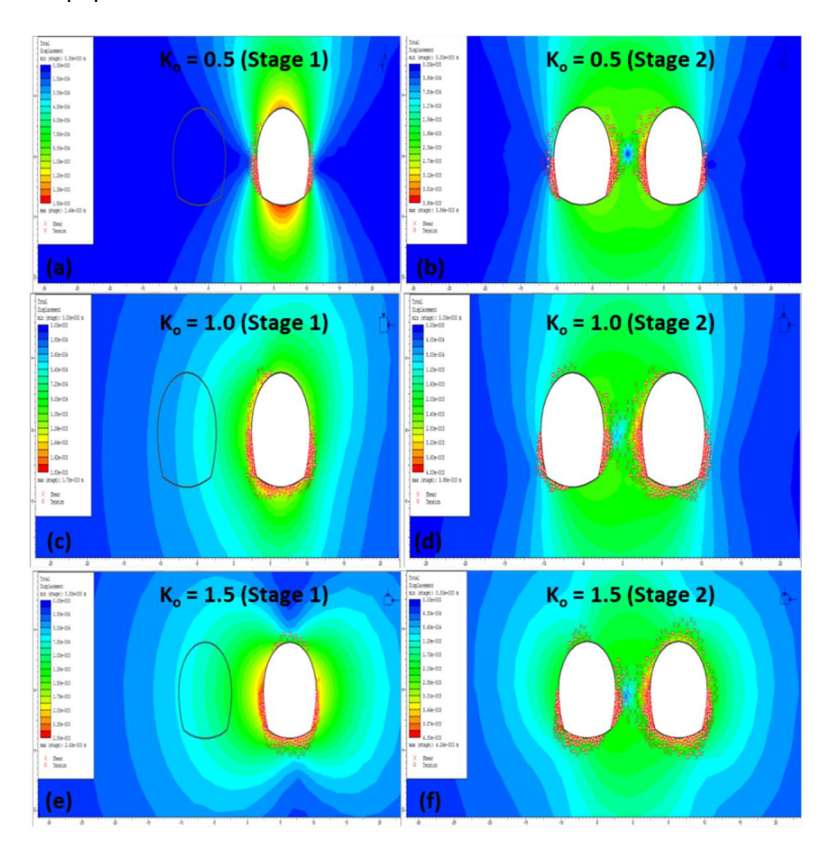


Fig. 6 Variation of displacements around interacting horse shoe tunnels in intact rock mass W/D 0.6

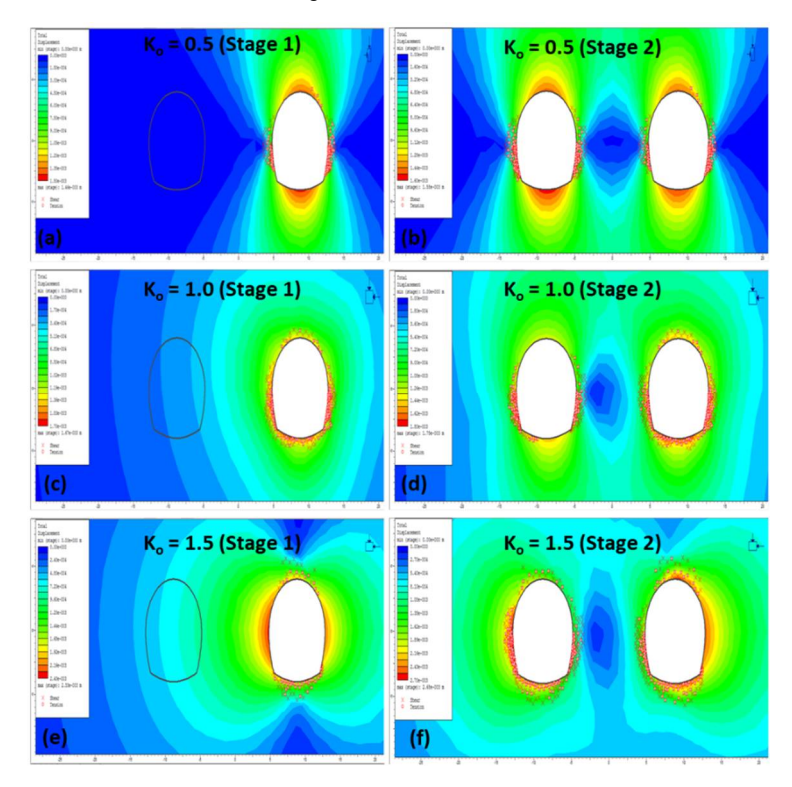


Fig. 7 Variation of displacements around sequentially excavated horse shoe tunnels in intact rock mass W/D 1.2

ISSN: 2229-7359 Vol. 11 No. 18s, 2025

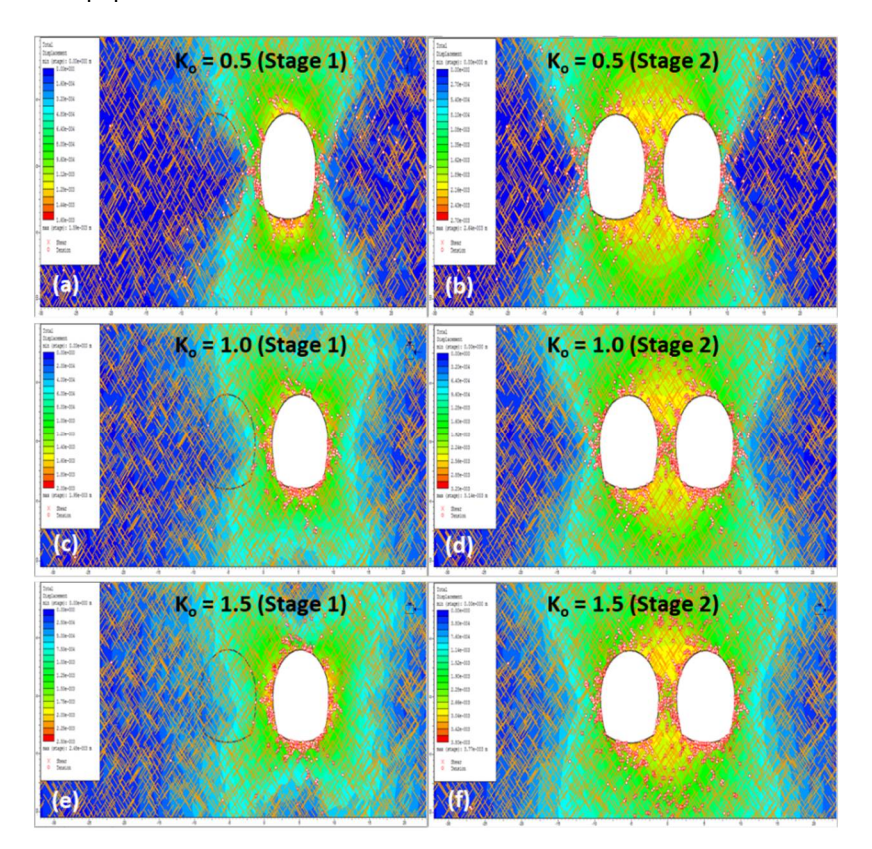


Fig. 8 Variation of displacements around sequentially excavated horse shoe tunnels in jointed rock mass W/D 0.3

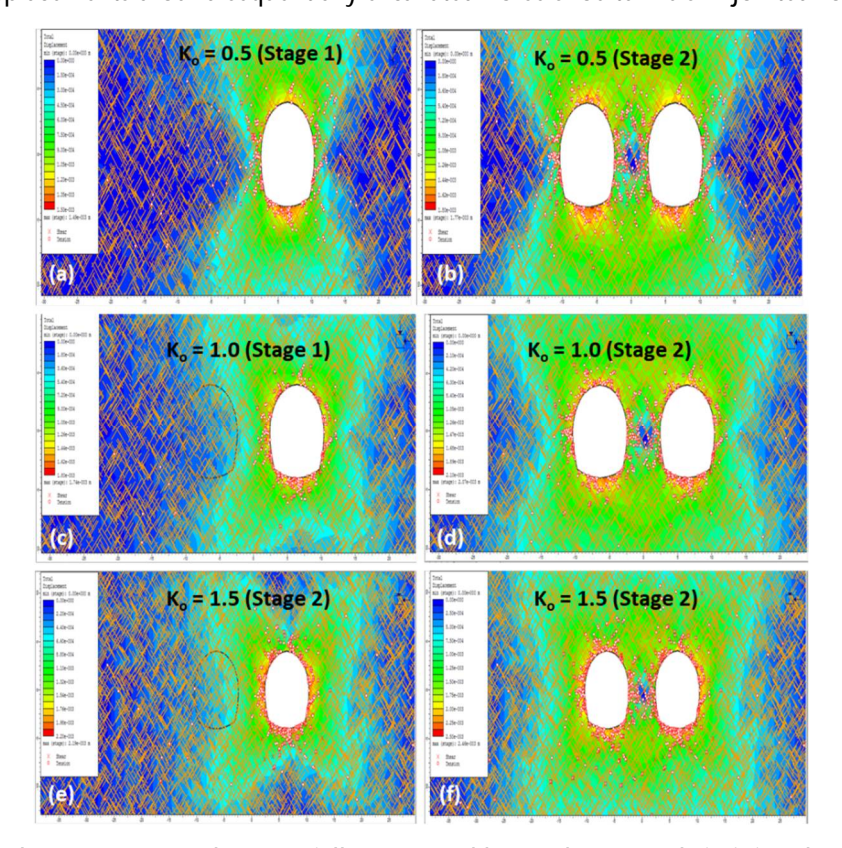


Fig. 9 Variation of displacements around sequentially excavated horse shoe tunnels in jointed rock mass W/D 0.6

mass and jointed rock mass when sequentially excavated

ISSN: 2229-7359 Vol. 11 No. 18s, 2025

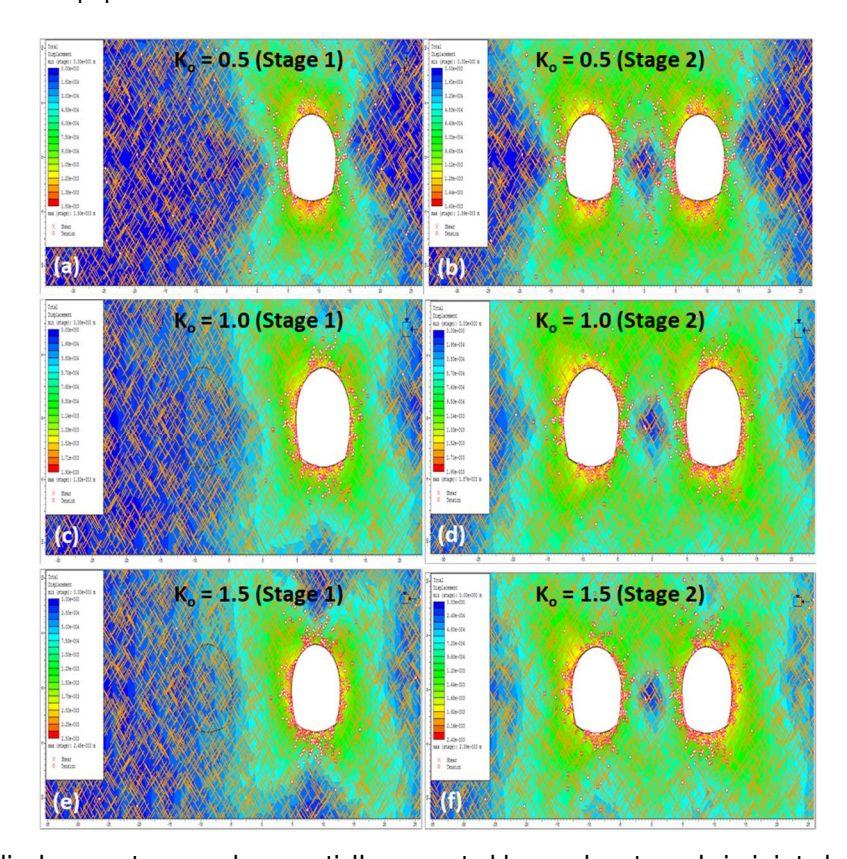


Fig. 10 Variation of displacements around sequentially excavated horse shoe tunnels in jointed rock mass W/D 1.2 **Table 3** Percentage difference in displacements at tunnel boundary and center of pillar zone between intact rock

	For the left tunnel								
Location	w/d =1.2			w/d=0.6			w/d=0.3		
	Ko 1.0	Ko 0.5	Ko 1.5	Ko 1.0	Ko 0.5	Ko 1.5	Ko 1.0	Ko 0.5	Ko 1.5
At springing level on pillar side	95.30	209.35	64.15	196.16	260.35	161.88	470.63	427.81	509.01
At crown	65.85	23.94	117.42	63.54	26.94	108.80	85.22	43.81	131.44
At springing level on abutment side	62.36	215.41	33.35	63.95	229.39	33.82	73.29	258.55	42.25
At invert level on abutment side	55.89	41.21	41.66	63.53	42.30	50.08	70.17	51.00	60.00
At center of invert	56.47	21.53	97.92	52.14	24.08	81.83	83.06	42.84	129.38
At invert level on pillar side	41.92	9.13	66.40	59.13	29.72	87.80	122.55	77.95	175.92
	At center of pillar								
At center of pillar zone	139.62	116.49	134.88	130.36	81.55	160.33	767.47	612.57	969.77

ISSN: 2229-7359 Vol. 11 No. 18s, 2025

https://theaspd.com/index.php

	For the right tunnel								
At springing level on pillar side	103.59	224.00	66.99	129.55	186.43	98.99	449.29	441.06	450.38
At crown	61.48	22.41	110.39	50.40	20.05	92.32	74.06	37.21	125.11
At springing level on abutment side	43.11	144.87	24.58	51.22	179.46	28.50	65.10	221.05	37.29
At invert level on abutment side	63.37	44.27	50.46	49.70	33.24	38.75	73.82	51.73	63.14
At center of invert	57.94	21.07	99.07	46.32	18.31	74.46	83.72	44.01	127.47
At invert level on pillar side	49.10	22.65	59.67	52.57	28.51	71.17	126.28	86.83	169.48

The graphical representations of results are shown in subsequent figures. (Fig. 11 to 14)

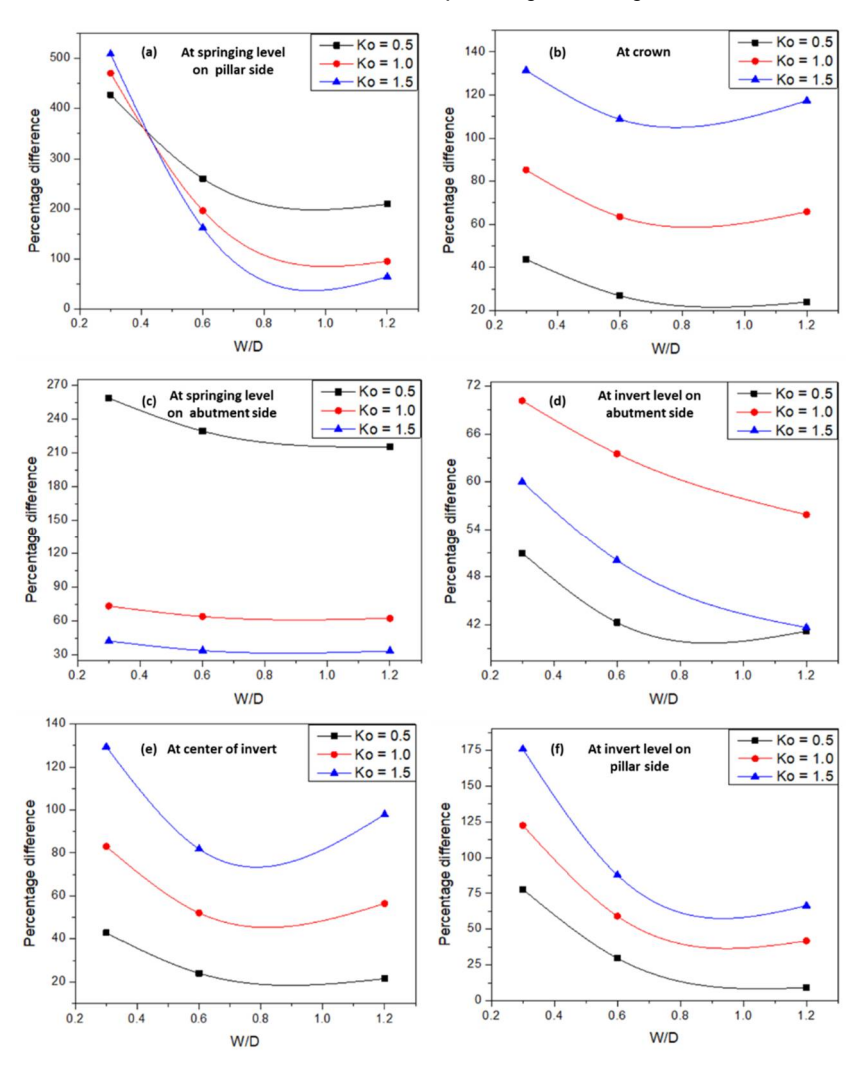


Fig. 11 Variation in percentage difference in deformation values between intact and jointed rock masses at boundary of tunnel for the left tunnel (JO=45/45)

ISSN: 2229-7359 Vol. 11 No. 18s, 2025

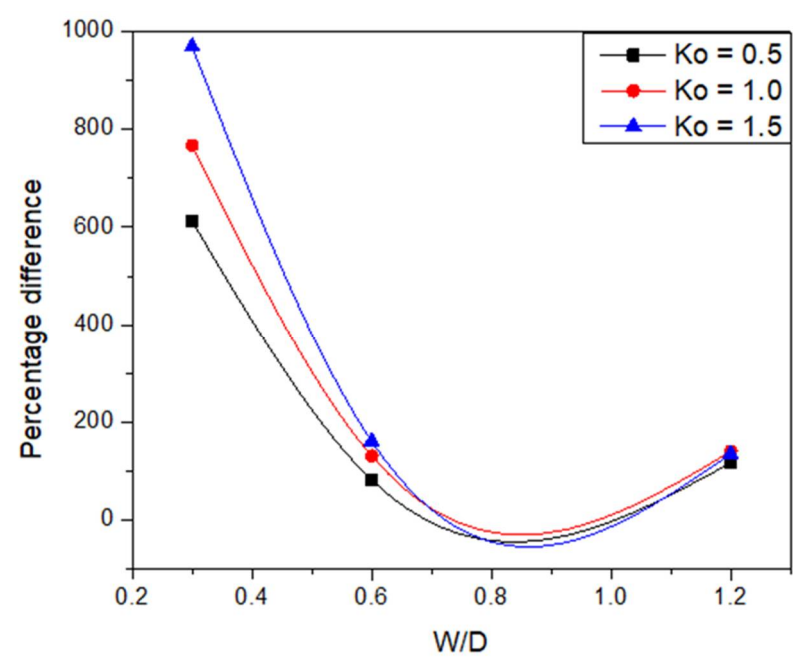


Fig. 12 Variation in percentage difference in deformation values between intact and jointed rock masses at at centre of pillar zone (JO=45/45)

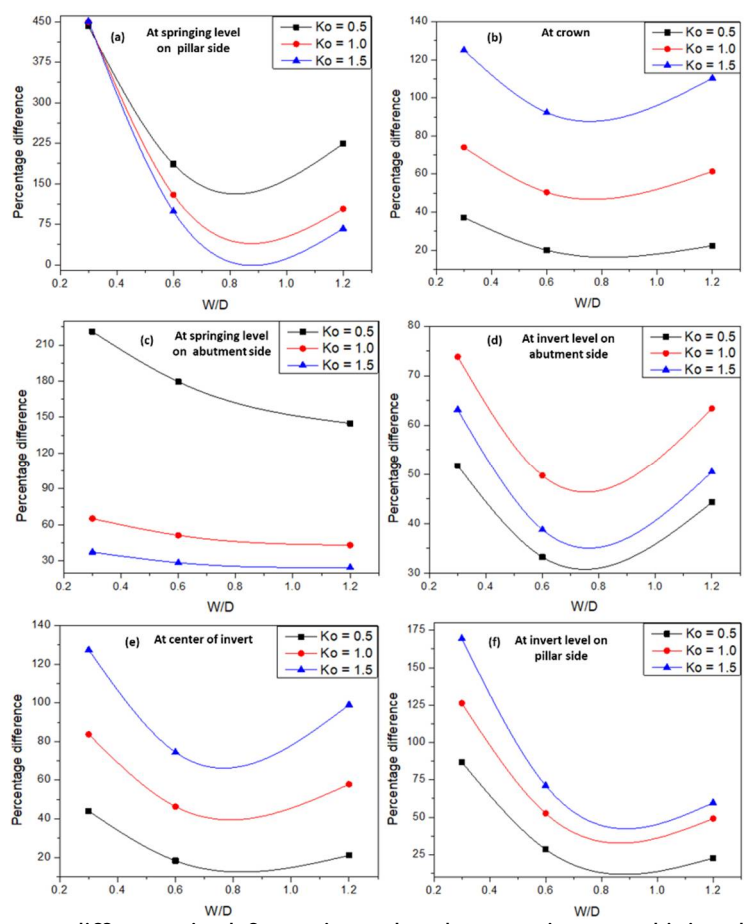


Fig. 13 Variation in percentage difference in deformation values between intact and jointed rock masses at boundary of tunnel for the right tunnel (JO=45/45).

ISSN: 2229-7359 Vol. 11 No. 18s, 2025

https://theaspd.com/index.php

4. At Springing Level on Abutment Side and Invert Level on Pillar Side:

The difference in percentage deformation at these locations shows a decreasing trend with increasing W/D ratio. At the springing level on the abutment side, the deformation decreases from 258.55 at W/D = 0.3 to 215.41 at W/D = 1.2. Similarly, at the invert level on the pillar side, the deformation decreases from 77.95 at W/D = 0.3 to 9.13 at W/D = 1.2. Fig. 11(c & f) This highlights the complex interaction between the twin tunnels and the surrounding rock mass.

At the center of the pillar zone

Results shows that the maximum difference in percentage deformation at the center of the pillar zone occurs under conditions of low W/D ratio (0.3) and high lateral earth pressure (Ko = 1.5) which is 969.77, while the minimum difference in deformation equal to 81.55 % occurs under conditions of high W/D ratio (1.2) and low lateral earth pressure (Ko = 0.5) fig 12.

The results indicate that the W/D ratio significantly influences the deformation behavior of twin parallel tunnels. Lower W/D ratios (0.3) generally lead to higher deformation, particularly at the springing level on the pillar side and the invert level on the abutment side. This is likely due to the increased stress concentration and reduced stability of the tunnel structure at smaller widths relative to depth.

1. Maximum Percentage Difference:

The highest percentage difference in deformation occurs at the springing level on the pillar side for the lowest W/D ratio (0.3) and the highest lateral earth pressure (Ko = 1.5). Specifically, at W/D = 0.3 and Ko = 1.5, the percentage difference in deformation reaches 450.38%, which is the maximum value observed in the dataset (fig. 13). This indicates that the difference in deformation between intact and jointed rock mass conditions is most pronounced at the springing level on the pillar side under conditions of low W/D ratio and high lateral earth pressure.

2. Minimum Percentage Difference:

The lowest percentage difference in deformation occurs at the invert level on the abutment side for the highest W/D ratio (1.2) and the lowest lateral earth pressure (Ko = 0.5). Specifically, at W/D = 1.2 and Ko = 0.5, the percentage difference in deformation is 33.24%, which is the minimum value observed in the dataset. This suggests that the difference in deformation between intact and jointed rock mass conditions is least significant at the invert level on the abutment side under conditions of high W/D ratio and low lateral earth pressure.

For right tunnel at 45-45:

1. At Springing Level on Pillar Side:

The percentage difference in deformation decreases as the W/D ratio increases. For example, at W/D = 0.3, the percentage difference is 450.38%, which decreases to 66.99% at W/D = 1.2. Fig. 13(a). This indicates that the difference in deformation between intact and jointed rock mass conditions is most significant at lower W/D ratios.

2. At Invert Level on Abutment Side:

The percentage difference in deformation also decreases with increasing W/D ratio. At W/D = 0.3, the percentage difference is 63.14%, which decreases to 50.46% at W/D = 1.2. Fig. 13(d). This suggests that the invert level on the abutment side experiences a smaller difference in deformation compared to the springing level on the pillar side.

ISSN: 2229-7359 Vol. 11 No. 18s, 2025

https://theaspd.com/index.php

3. At Crown and Centre of Invert:

The percentage difference in deformation at the crown and centre of invert levels shows a decreasing trend with increasing W/D ratio. For example, at the crown, the percentage difference decreases from 125.11% at W/D = 0.3 to 110.39% at W/D = 1.2. Similarly, at the centre of invert, the percentage difference decreases from 127.47% at W/D = 0.3 to 99.07% at W/D = 1.2. Fig. 13(b & e).

4. At Springing Level on Abutment Side and Invert Level on Pillar Side:

The percentage difference in deformation at these locations also decreases with increasing W/D ratio. At the springing level on the abutment side, the percentage difference decreases from 37.29% at W/D = 0.3 to 24.58% at W/D = 1.2. At the invert level on the pillar side, the percentage difference decreases from 169.48% at W/D = 0.3 to 59.67% at W/D = 1.2. Fig 13 (c & f).

4. Conclusions

This conclusion summarizes the key findings and their implications for tunnel design, focusing on the influence of W/D ratios, in-situ stress conditions, and rock mass properties.

1. W/D Ratio Influence:

Lower W/D ratios (e.g., 0.3) result in higher percentage deformation differences between intact and jointed rock masses, particularly at critical locations like the springing level on the pillar side and center of the pillar zone (509.01% and 969.77% respectively).

Higher W/D ratios (e.g., 1.2) significantly reduce deformation differences, indicating diminished interaction effects between the tunnels showing minimum values as low as 9.13% and 21.07% at invert level on pillar side and centre of invert respectively at Ko=0.5).

2. Maximum Deformation Difference:

The center of the pillar zone exhibits the highest deformation difference, reaching 969.77% at W/D = 0.3 and $K_0 = 1.5$, highlighting the severe stress concentration at smaller pillar widths.

3. Minimum Deformation Difference:

The invert level on the abutment side shows the least deformation difference, with values as low as 9.13% at W/D = 1.2 and $K_0 = 0.5$, indicating reduced stress impact at larger pillar widths.

4. In-Situ Stress (K₀) Impact:

Higher K_0 values (e.g., 1.5) amplify deformation differences, especially at lower W/D ratios, while lower K_0 values (e.g., 0.5) result in reduced deformation differences.

5. Critical Locations:

The springing level on the pillar side and center of the pillar zone are the most sensitive to deformation, with differences exceeding 400% at W/D = 0.3 and $K_0 = 1.5$.

ISSN: 2229-7359 Vol. 11 No. 18s, 2025

https://theaspd.com/index.php

Design Recommendations: To mitigate stress concentration and deformation risks, avoid W/D ratios < 0.5 in high-stress conditions ($K_0 \ge 1.0$), as they can lead to deformation differences exceeding 500% in jointed rock masses. Instead, adopt W/D ratios ≥ 1.0 for tunnels in weak or jointed rock, which reduce interaction effects and keep deformation differences below 25%, ensuring minimal stress overlap and enhanced stability. Also, the center of the pillar zone and springing level (pillar side) are critical areas requiring prioritized reinforcement (e.g., rock bolts, shotcrete) when W/D < 0.75, as deformation differences can exceed 900% under high-stress conditions ($K_0 \ge 1.5$). For tunnels in high in-situ stress ($K_0 > 1.2$), increase the W/D ratio to ≥ 0.75 or use yielding supports to manage deformations, whereas in low-stress conditions ($K_0 \le 0.5$), a W/D ≥ 1.0 ensures minimal interaction effects with deformation differences below 10%.

References

- [1] Franza, A. and DeJong, M. J. (2019). "Elastoplastic solutions to predict tunneling-induced load redistribution and deformation of surface structures." Journal of Geotechnical and Geoenvironmental Engineering, 145(4), 04019007.
- [2] Varma, M., Maji, V.B. and Boominathan, A. (2019). "Numerical modeling of a tunnel in jointed rocks subjected to seismic loading." Underground Space, 4(2), 133-146.
- [3] Zhang, W., Xu, B., Mei, J., Yue, G. and Shi, W. (2020). "A numerical study on mechanical behavior of jointed rock masses after tunnel excavation." Arabian Journal of Geosciences, 13, 416.
- [4] Zhang, J., Chen, J., Wang, J. and Zhu, Y. (2020). "Failure modes of tunnels in jointed rock masses." Tunnelling and Underground Space Technology, 97, 103-115.
- [5] Huang, X., Zhang, J., Yang, L. and Yang, S. (2016). "Elasto-plastic analysis of the surrounding rock mass in circular tunnel based on the generalized nonlinear unified strength theory." International Journal of Mining Science and Technology, 26(5).
- [6] Fang, Q., Tai, Q., Zhang, D. and Wong, L.N.Y. (2016). "Ground surface settlements due to construction of closely-spaced twin tunnels with different geometric arrangements." Tunnelling and Underground Space Technology, 51, 144-151.
- [7] Fu, J., Yang, J., Yan, L. and Abbas, S. M. (2015). "An analytical solution for deforming twin-parallel tunnels in an elastic half plane." International Journal for Numerical and Analytical Methods in Geomechanics, 39, 524-538.
- [8] Satici, O. and Unver, B. (2015). "Assessment of tunnel portal stability at jointed rock mass: A comparative case study." Computers and Geotechnics, 64, 72–82.
- [9] Salim, N. M. (2013). "Interaction between the existing and the new constructed tunnels." Engineering and Technology Journal, 31(19).
- [10] Sahoo, J.P. and Kumar, J. (2013). "Stability of long unsupported twin circular tunnels in soils." Tunnelling and Underground Space Technology, 38, 326-335.
- [11] Huang, X., Schweiger, H.F. and Huang, H. (2013). "Influence of deep excavations on nearby existing tunnels." International Journal of Geomechanics, 13(2), 170-180.
- [12] Melkoumian, N., Priest, S.D. and Hunt, S.P. (2009). "Further development of the three-dimensional Hoek-Brown yield criterion." Rock Mechanics and Rock Engineering, 42(6), 835–847.
- [13] Lee, S.D. and Kim, I. (2009). "Behavior of tunnel due to adjacent ground excavation under the influence of pre-loading on braced wall." Geotechnical Aspects of Underground Construction in Soft Ground.
- [14] Singh, M., Singh, B. and Choudhari, J. (2007). "Critical strain and squeezing of rock mass in tunnels." Tunnelling and Underground Space Technology, 22(3), 343-350.

ISSN: 2229-7359 Vol. 11 No. 18s, 2025

- [15] Sun, J.S., Lu, W.B., Zhu, Q.H. and Chen, M. (2007). "Elasto-plastic analysis of circular tunnels in jointed rock masses satisfying the Hoek-Brown failure criterion." Journal of China University of Mining and Technology, 17(3), 393-398.
- [16] Karakus, M., Ozsan, A. and Basarir, H. (2007). "Finite element analysis for the twin metro tunnel constructed in Ankara Clay, Turkey." Bulletin of Engineering Geology and the Environment, 66(1), 71-79.
- [17] Chehade, F. H. and Shahrour, I. (2008). "Numerical analysis of the interaction between twin-tunnels: Influence of the relative position and construction procedure." Tunnelling and Underground Space Technology, 23, 210–214.
- [18] Chakeri, H., Hasanpour, R., Hindistan, M.A. and Unver, B. (2011). "Analysis of interaction between tunnels in soft ground by 3D numerical modeling." Bulletin of Engineering Geology and the Environment, 70, 439–448.
- [19] Alejano, L.R. and Bobet, A. (2012). "Drucker-Prager Criterion." Rock Mechanics and Rock Engineering, 45, 995–999.
- [20] Hoek, E., Carranza-Torres, C. and Corkum, B. (2002). "Hoek-Brown failure criterion 2002 edition." Proceedings of NARMS-TAC, Toronto, Canada.
- [21] Misra, A. (2002). "Effect of asperity damage on shear behavior of single fracture." Engineering Fracture Mechanics, 69(17), 1997-2014.
- [22] Karakus, M. and Fowell, R.J. (2003). "Effects of different tunnel face advance excavation on the settlement by FEM. Tunnelling and Underground Space Technology, 18(5), 513–523.
- [23] Carranza-Torres, C. (2003). "Dimensionless graphical representation of the exact elastoplastic solution of a circular tunnel in a Mohr-Coulomb material subject to uniform far-field stresses." Rock Mechanics and Rock Engineering, 36(3), 237-253.
- [24] Asano, T., Ishihara, M., Kiyota, Y., Kurosawa, H. and Ebisu, S. (2003). "An observational excavation control method for adjacent mountain tunnels." Tunnelling and Underground Space Technology, 18, 291–301.
- [25] Bhasin, R. and Hoeg, K. (1997). "Numerical modelling of block size effects and influence of joint properties in multiply jointed rock." Tunnelling and Underground Space Technology, 12(3), 407-415.
- [26] Shen, B. and Barton, N. (1997). "The effect of joint spacing on the stability of underground openings." International Journal of Rock Mechanics and Mining Sciences, 34(3–4), 419–435.
- [27] Grimstad, E. and Bhasin, R. (1999). "Rock support in hard rock tunnels under high stress. Norwegian Geotechnical Institute, Report 205.
- [28] Hoek, E. (1994). "Strength of rock and rock masses." ISRM News Journal, 2(2), 4-16.
- [29] Hoek, E. and Brown, E.T. (1988). "The Hoek-Brown failure criterion—a 1988 update." Proc. 15th Canadian Rock Mechanics Symposium.
- [30] Barton, N. (1995). "General Outline of Norwegian Method of Tunnelling." Tunnels and Underground, 26(10), 39-46.
- [31] Srivastava, R. K. (1985). "Elasto-Plastic Finite Element Analysis of Interacting Tunnels." PhD Thesis, Indian Institute of Technology, Delhi.
- [32] Ghaboussi, J. AND RANKEN, R. E. (1977). "INTERACTION BETWEEN TWO PARALLEL TUNNELS" INTERNATIONAL JOURNAL FOR NUMERICAL AND ANALYTICAL METHODS IN GEOMECHANICS. VOL. 1. 75-103 0977).
- [33] Huang, X., Schweiger, H. F., and Huang, H. (2016). "A Versatile Strength Theory for Elasto-Plastic Analysis of Tunnel Surrounding Rock." International Journal of Rock Mechanics and Mining Sciences, 83, 1-12.
- [34] Franza, A., and DeJong, M. J. (2019). "Tunneling-Induced Soil-Structure Interaction: A Two-Stage Elasto-Plastic Analysis Method." Computers and Geotechnics, 110, 1-14.

ISSN: 2229-7359 Vol. 11 No. 18s, 2025

- [35] Varma, M., Singh, T. N. and Singh, V. (2019). "Response of Tunnels in Jointed Rock Masses Under Dynamic Loading: An Experimental and Numerical Study." Rock Mechanics and Rock Engineering, 52(11), 4567-4585.
- [36] Khan, I. A., Venkatesh, K. and Srivastava, R. K. (2021). Elasto-plastic finite element analysis of twin tunnels A comparison of excavation in intact and jointed rock mass. Materials Today: Proceedings https://doi.org/10.1016/j.matpr.2021.05.122.
- [37] Wang, H. N., Chen, X. P., Jiang, M. J., Song, F., & Wu, L. (2018). "The analytical predictions on displacement and stress around shallow tunnels subjected to surcharge loadings." Tunnelling and Underground Space Technology, 71, 403–427. https://doi.org/10.1016/j.tust.2017.09.015.
- [38] N. Barton, Int. J. Rock Mech. Min. Sci. Geomech. Abstr., 9(5) (1972) 579-602.
- [39] V. choubey, Rock Mech. 10(1-2) (1972) 1-54.
- [40] Z.T. Bieniawski, Engineering Rock Mass Classifications, Wiley, New York, 1989.
- [41] Lin, Q., Cao, P., Meng, J., Cao, R. and Zhao, Z. (2020). Strength and failure characteristics of jointed rock mass with double circular holes under uniaxial compression: Insights from discrete element method modelling. *Theoretical and Applied Fracture Mechanics*, 109, 102692. https://doi.org/10.1016/j.tafmec.2020.102692.
- [42] 42. Fan, X., Lin, H., Lai, H., Cao, R. and Liu, J. (2018). Numerical analysis of the compressive and shear failure behavior of rock containing multi-intermittent joints. *Comptes Rendus. Mécanique*, *347*(1), 33–48. https://doi.org/10.1016/j.crme.2018.11.001.